# Analysis of Anti-Stokes Resonance Raman Excitation Profiles as a Method for Studying Vibrationally Excited Molecules

**Hiromi Okamoto,* Takakazu Nakabayashi, and Mitsuo Tasumi**

*Research Centre for Spectrochemistry and Department of Chemistry, School of Science, The University of Tokyo, Bunkyo-ku, Tokyo 113, Japan*

*Received: October 24, 1996; In Final Form: January 31, 1997*[⊗]

Anti-Stokes and Stokes resonance Raman excitation profiles have been observed for the C=C and C−C stretching fundamental bands of carotenoids ($\beta$-carotene and canthaxanthin) and analyzed on the basis of the Franck−Condon mechanism. It is shown that such an analysis provides a method for identifying the vibrational levels on which vibrationally excited molecules observed in picosecond pump−probe processes are populated.

## Introduction

Over the past two decades, a number of studies have been devoted to the analyses of Raman excitation profiles (REPs), that is, excitation wavelength dependencies of resonance Raman intensities (usually in the Stokes side). It is now established that the analysis of an REP is useful for clarifying the mechanism of the resonance Raman process under study on the basis of the convenient formulation by Albrecht,[1,2] which states that the resonance Raman processes are mainly due to either the A term (Franck−Condon mechanism) or the B term (vibronic coupling mechanism). From detailed analyses of REPs, it is possible to derive valuable information on molecular structures in excited electronic states.[3−11]

Developments in transient and time-resolved Raman spectroscopy have enabled us to obtain the Raman spectra of short-lived excited species. One of the present authors (MT) has reported[12] with coauthors the observation of the picosecond time-resolved anti-Stokes Raman spectra of vibrationally excited carotenoids generated via relaxation from electronically excited states. From picosecond anti-Stokes Raman intensity changes, electronically excited carotenoids have been found to relax nonradiatively to vibrationally excited states of the ground electronic state within ∼10 ps. In order to discuss the mechanism of vibrational relaxation, it is important to identify the energy levels on which the vibrationally excited molecules generated via relaxation from excited electronic states are populated.

Anti-Stokes Raman scattering arises from vibrationally excited molecules. Since the populations of molecules in excited vibrational states are very small at room temperature (with the exception of those for low-frequency modes), anti-Stokes Raman bands are generally very weak. For example, if we assume the Boltzmann distribution, the population in an excited vibrational state at 1000 $cm^{-1}$ is only ∼1/150 of that of the ground state and ∼1/1800 for an excited state at 1500 $cm^{-1}$. So far, experimental analysis of anti-Stokes excitation profiles is limited to vibrational modes with relatively low vibrational frequencies.[13] However, recent multichannel Raman spectrometers equipped with liquid nitrogen cooled charge-coupled device (CCD) systems are so sensitive that anti-Stokes Raman spectra in the region below ∼1600 $cm^{-1}$ can be observed from samples at room temperature with sufficiently high signal-to-noise ratios.

The purpose of the present paper is to observe REPs for the cw-excited anti-Stokes scattering from carotenoids (*all-trans*-$\beta$-carotene and *all-trans*-canthaxanthin) at room temperature as well as for the Stokes scattering from the same carotenoids and to examine the possibility of utilizing the results obtained to the identification of the energy states of vibrationally excited molecules observed in recent pump−probe measurements.[12]

## Experimental Section

Anti-Stokes Raman measurements were performed on a multichannel Raman spectrometer with visible excitation lines. Raman spectra were excited with seven lines (514.5, 496.5, 488.0, 476.5, 472.7, 465.8, and 457.9 nm) from an $Ar^+$ laser (Coherent Innova 90), the second harmonic (532.1 nm) of a cw Q-switched Nd:YAG laser (Quantronix 532F-O/QS-2), and a tunable output from a synchronously-pumped mode-locked dye laser (Spectra-Physics/Quantronix 3500, 542−590 nm) excited by the second harmonic of a cw mode-locked Nd:YLF laser (Quantronix 4216D). The latter two kinds of light were obtained as short pulses (∼100 ns for the Q-sw Nd:YAG laser and ∼5 ps for the dye laser). The gain medium of the dye laser was an ethylene glycol solution of rhodamine 560 or rhodamine 590. It is established that carotenoids recover their initial spectra within 100 ps after visible photoexcitation,[12] and no major relaxation process with a longer time scale is known. In this case, spectral changes due to re-excitation of previously pumped molecules are negligible if the peak power of the excitation light source is sufficiently low (minor changes may occur, owing to a small temperature increase). In the present experiment, the average power of the exciting light was 5−80 mW at the sample position, and the peak power of that was limited to less than 100 W for the pulsed sources. The beam diameter of the exciting light was >0.3 mm at the sample point. Under this condition, spectral changes due to the re-excitation of molecules are negligible.

The sample solution was contained in a rotating cell at room temperature. The 90° scattering geometry was adopted. The Raman scattered light was analyzed by a triple polychromator (Spex Triplemate 1877) and detected by a liquid nitrogen cooled CCD detector (Princeton Instruments LN/CCD-1752PBUVAR). Sensitivity differences between pixels of the CCD detector were found to be less than 10% by the spectral measurement of white light from a tungsten lamp. Dependence of the sensitivity of the spectrograph on the wavelength of scattered light was corrected[14] by using rotational Raman spectra of deuterium ($D_2$). The spectral slit width was set at 10−15 $cm^{-1}$. The incident

* To whom correspondence should be addressed. E-mail: kh4h-okmt@asahi-net.or.jp or aho@chem.s.u-tokyo.ac.jp.

[⊗] Abstract published in *Advance ACS Abstracts,* April 1, 1997.

S1089-5639(96)03302-6 CCC: $14.00 

laser radiation was linearly polarized, and neither a polarizer nor a polarization scrambler (depolarizer) was used to keep the throughput of the spectrometer as high as possible. Polarization dependency of the sensitivity of the spectrograph was separately examined by using the Raman bands of cyclohexane, and the intensity data were corrected on the basis of the measured polarization characteristics. Peak positions (Raman shifts) in the Raman spectra excited with the 514.5-nm line were calibrated by reference lines from a Ne lamp.

*all-trans*-$\beta$-Carotene was purchased from the Wako Pure Chemical Industries and recrystalized from a benzene−methanol mixture. *all-trans*-Canthaxanthin was purchased from Extrasynthèse and used as received. We chose benzene as a solvent. In benzene solution, the carotenoids show the 0−0 absorption maximum at a relatively long wavelength (∼500 nm). This situation is convenient for using an $Ar^+$ laser and a dye laser as excitation light sources. Benzene shows a very strong totally symmetric Raman band at 992 $cm^{-1}$, which can be used as an internal intensity reference. Since other Raman bands from benzene are far weaker than the 992 $cm^{-1}$ band, they do not seriously interfere with the Raman bands of the carotenoids. Unfortunately, the carotenoids show a Raman band at around 1000 $cm^{-1}$, which overlaps with the 992 $cm^{-1}$ band of benzene. The overlapping bands from benzene and the carotenoids were numerically separated by a method to be described later. The concentration of the sample solution was $10^{-4}$−$10^{-5}$ mol $dm^{-3}$. Electronic absorption spectra were recorded on a Hitachi U-3500 spectrophotometer. The electronic absorption spectra of the carotenoids showed no concentration dependence in the range of concentration employed for the Raman measurements.

## Analysis

**Determination of relative Raman Intensities.** Relative Raman intensities are usually determined by dividing the band intensities of the solute by the intensity of a solvent band (internal intensity reference) and the concentration of the solute. As mentioned earlier, however, the 992 $cm^{-1}$ band of benzene, which is to be used as the internal intensity reference, overlaps with the Raman band of the carotenoids at ∼1000 $cm^{-1}$. Then, the simple method mentioned above is not applicable in the present case. To solve this problem, the Raman spectra of sample solutions with two different concentrations were observed and utilized to separate the contribution of the solute and that of the solvent by the method described below.

As is well-known, the absorbance $A$ of an absorption band is proportional to the concentration $c$ of an absorbing solute in solution and the optical pathlength $l$. Thus, $A$ is given as

$$A = \epsilon c l \tag{1}$$

where $\epsilon$ is the molar absorption coefficient of the solute.

The Raman band of the solute and that of the solvent are assumed to overlap at a Raman shift $\nu_a$. Then, the Raman intensity $I_a$ observed at $\nu_a$ is given by the following equation:

$$I_a = k(s + \alpha c) \tag{2}$$

where $s$ is the absolute Raman intensity from the solvent at $\nu_a$; $\alpha$ is the absolute Raman intensity per unit concentration from the solute (carotenoid) at $\nu_a$; and $k$ is a proportionality constant determined by the conditions of Raman measurement. On the other hand, it is assumed that only the solute contributes to the Raman intensity $I_b$ at another Raman shift $\nu_b$. The Raman intensity observed at $\nu_b$ is then given by

$$I_b = k\beta c \tag{3}$$

where $\beta$ is the absolute Raman intensity per unit concentration from the solute at $\nu_b$.

To obtain the REPs of bands at $\nu_a$ and $\nu_b$ from the solute, it is necessary to have appropriate expressions for $\alpha/s$ and $\beta/s$, or quantities which are proportional to them. If no Raman band from the solute overlaps with that from the solvent at $\nu_a$, i.e., $\alpha = 0$, a quantity proportional to $\beta/s$ for the Raman band at $\nu_b$ can be obtained by dividing $I_b$ by the product of $I_a$ and $A$. If $\alpha \neq 0$, the following treatment based on the absorption and Raman measurements at two different sample concentrations, $c_1$ and $c_2$, becomes necessary to obtain the above quantities. In this case, the above equations may be rewritten as follows:

$$A_1 = \epsilon c_1 l \tag{4a}$$

$$A_2 = \epsilon c_2 l \tag{4b}$$

where $A_1$ and $A_2$ represent the absorbances of the first and second solutions, respectively. As for the Raman intensities

$$I_{a1} = k_1(s + \alpha c_1) \tag{5a}$$

$$I_{a2} = k_2(s + \alpha c_2) \tag{5b}$$

and

$$I_{b1} = k_1\beta c_1 \tag{6a}$$

$$I_{b2} = k_2\beta c_2 \tag{6b}$$

where $I_{a1}$ and $I_{a2}$ denote, respectively, the Raman intensities of the first and second solutions at $\nu_a$, and $I_{b1}$ and $I_{b2}$ those at $\nu_b$. In eqs 5 and 6, we have used different $k$ values for the first and second solutions ($k_1$ and $k_2$) to take into account changes in laser power and detection sensitivity in the measurements of the two solutions. Equations 4−6 lead to the following expressions for $\alpha/(s\epsilon l)$ and $\beta/(s\epsilon l)$:

$$\frac{\alpha}{s\epsilon l} = \frac{\dfrac{I_{b1}I_{a2}}{A_1} - \dfrac{I_{b2}I_{a1}}{A_2}}{I_{b2}I_{a1} - I_{b1}I_{a2}} \tag{7a}$$

$$\frac{\beta}{s\epsilon l} = I_{b1}I_{b2}\frac{\dfrac{I}{A_1} - \dfrac{1}{A_2}}{I_{b2}I_{a1} - I_{b1}I_{a2}} \tag{7b}$$

REPs are obtained by plotting the quantities in eqs 7a and 7b against the excitation wavelength. Errors may accumulate in the above computations, especially for $\alpha/(s\epsilon l)$, which corresponds to the absolute Raman intensity of the solute at ∼1000 $cm^{-1}$. Therefore, only the REPs of the Raman bands at ∼1520 and ∼1160 $cm^{-1}$ of the solute, which correspond to $\beta/(s\epsilon l)$ in eq 7b, are analyzed.

Effects of reabsorption of the scattered light by the solution itself are corrected[3] on the basis of the observed absorption spectra with a value of 0.7 mm for the effective pathlength of the scattered light. The total errors in the observed Raman intensities are estimated to be ∼15% for the Stokes bands and ∼30% for the anti-Stokes bands.

**Simulation of REPs.** The observed Stokes and anti-Stokes REPs are compared with the results of calculation based upon the A term of Albrecht's formula (Franck−Condon mechanism).[1,2] We assume that broadening of the electronic absorption band can be expressed by a simple convolution of homogeneous and inhomogeneous broadening functions,[5,6] which are Lorentzian and Gaussian, respectively. According

to analyses of the resonance Raman and fluorescence spectra of carotenoids on the stochastic theory,[9,10,15] solute−solvent interaction, which causes fluctuation of the electronic transition energy, is in the slow modulation regime (or static limit). This rationalizes the above-mentioned expression of the electronic absorption band shape. We do not adopt the transform theory,[16] which is used to transform an electronic absorption spectrum into Raman excitation profiles. The goal of this paper is to predict anti-Stokes Raman excitation profiles for various vibrationally excited transients. For this purpose, we cannot apply the transform theory because it is almost impossible to obtain electronic absorption spectra from well-defined vibrationally excited states.

The *zz*-component of homogeneously broadened Raman tensor, $a_{zz}(\nu_0)$, for the $f \leftarrow i$ transition from the initial ($i$) state to the final ($f$) state with the excitation frequency $\nu_0$ is proportional, within the framework of the Kramers−Heisenberg−Dirac formulation,[17]

$$a_{zz}(\nu_0) \approx \sum_{v} \frac{\langle f|v\rangle\langle v|i\rangle}{\Delta E_{vi} - h\nu_0 + i\Gamma} \tag{8}$$

where $v$ represents a virtual state; $\Delta E_{vi}$ is the energy difference between the virtual and initial states; and $\Gamma$ is the homogeneous half-width. In the Raman spectra of carotenoids with visible excitation, it is known that the Raman tensor components other than $a_{zz}$ has only small contribution to Raman intensities.[18] The Raman intensity in photon numbers (not in radiation energy), $I_{f\leftarrow i}(\nu_0)$, including the inhomogeneous broadening, is given by

$$I_{f\leftarrow i}(\nu_0) \approx (\nu_0 - \nu_{f\leftarrow i})^3 G(\nu') * |a_{zz}(\nu_0)|^2$$

$$G(\nu') = \exp[-4 \ln 2\, (\nu'/\nu_{IH})^2] \tag{9}$$

where $G(\nu')$ is the inhomogeneous broadening function; the symbol $*$ represents the convolution of two functions; $\nu_{IH}$ denotes the inhomogeneous half-width; and $\nu_{f\leftarrow i}$ is the Raman shift in frequency. (Therefore, $\nu_0 - \nu_{f\leftarrow i}$ corresponds to the frequency of the scattered Raman light.)

For the calculation of the Franck−Condon factors, three strongly Raman-active normal coordinates for the C=C stretch, C−C stretch, and $CH_3$ rock are considered. For the sake of simplicity, we assume that the intramolecular potential functions are harmonic and of the same shape for the ground and optically allowed excited electronic states and that the Duschinsky rotation[19] is negligibly small. The Franck−Condon factor in eq 8 is then given by the following form

$$\langle v|i\rangle = \prod_m \int \psi_{i_m}(\xi_m)\, \psi_{v_m}(\xi_m - \Delta_m)\, d\xi_m \tag{10}$$

where $\psi_i$ represents the eigenfunction of a harmonic oscillator with the quantum number $i$, and $\xi_m$ is the dimensionless coordinate for the $m$th normal mode ($m = 1-3$ for the C=C stretch, C−C stretch, and $CH_3$ rock, respectively). The dimensionless displacements, $\Delta_m$'s, between the equilibrium positions of the ground and excited states along the above-mentioned normal coordinates are adjusted to obtain the best fits between the calculated and experimental REPs. As for the $CH_3$ rock, the displacement parameter $\Delta_3$ was fixed at 0.6, in view of the results of previous studies.[3−10] Summation over the virtual states was performed for 100 virtual states, which give the three-dimensional Franck−Condon factors from the largest to 100th in magnitude.

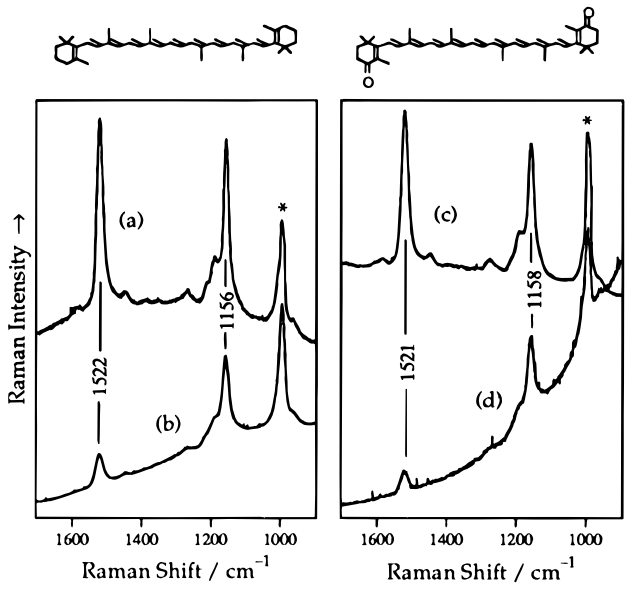


**Figure 1.** (Top) Chemical structures of carotenoids studied; $\beta$-carotene (left) and canthaxanthin (right). (Bottom) Typical Stokes and anti-Stokes Raman spectra of carotenoids in benzene solutions. (a) $\beta$-Carotene ($\sim 6 \times 10^{-5}$ mol dm$^{-3}$), Stokes spectrum excited at 514.5 nm. (b) $\beta$-Carotene ($\sim 6 \times 10^{-5}$ mol dm$^{-3}$), anti-Stokes spectrum excited at 542 nm. (c) Canthaxanthin ($\sim 2 \times 10^{-5}$ mol dm$^{-3}$), Stokes spectrum excited at 514.5 nm. (d) Canthaxanthin ($\sim 4 \times 10^{-5}$ mol dm$^{-3}$), anti-Stokes spectrum excited at 542 nm. The bands marked with an asterisk have contributions from the 992 cm$^{-1}$ band of benzene.

Similarly, the electronic absorption spectra are simulated by the following equation:

$$A(\nu_0) \sim G(\nu') * [\sum_{v} \Delta E_{vi} |\langle v|i\rangle|^2 L_v(\nu_0)]$$

$$L_v(\nu_0) = \frac{1}{(\Delta E_{vi} - h\nu_0)^2 + \Gamma^2} \tag{11}$$

This is based upon the Franck−Condon principle, and the electronic transition is assumed to be broadened by both the homogeneous [Lorentzian, $L_v(\nu_0)$] and inhomogeneous [Gaussian, $G(\nu')$] mechanisms. The calculation was performed with the same parameters of potential displacements and electronic band broadening as used in the calculation of Stokes and anti-Stokes REPs.

## Results and Discussion

**Observed and Simulated Excitation Profiles.** In Figure 1, the typical Stokes and anti-Stokes resonance Raman spectra of $\beta$-carotene and canthaxanthin are shown. The Stokes spectra (Figure 1a,c) agree well with those reported previously. The three strong bands at ~1520, ~1160, and ~1000 cm$^{-1}$ (the last one overlapping with the band of benzene at 992 cm$^{-1}$) are assigned, respectively, to the C=C stretch, C−C stretch, and $CH_3$ rock.[18] The anti-Stokes spectra (Figure 1b,d) are essentially the same as the Stokes spectra, except that the band intensities decrease with increasing Raman shift, reflecting the Boltzmann distribution of molecules in the initial states. The background signal of the anti-Stokes spectra, which is strong in the low-frequency region, may be due to fluorescence from the sample (and impurities) as well as the background emission from the dye laser. Attempts to observe overtone and combination spectra in the region higher than 2000 cm$^{-1}$ were made; however, only very weak signals not suitable for quantitative analyses were obtained. Populations in the vibrational states

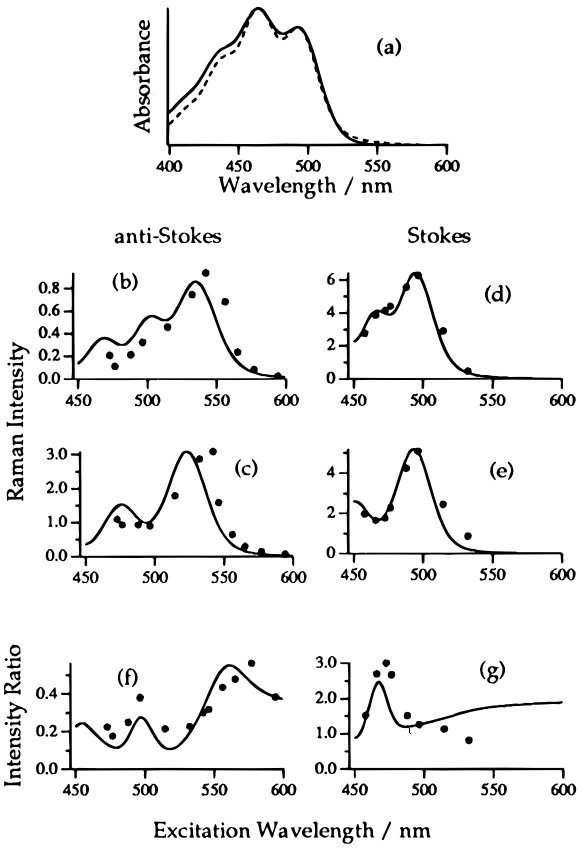


**Figure 2.** Electronic absorption spectrum and Raman excitation profiles of $\beta$-carotene in benzene solution. (a) Electronic absorption spectrum: observed (solid curve) and simulated (broken curve). (b, c) Anti-Stokes excitation profiles of the bands at 1522 (b) and 1156 $cm^{-1}$ (c). (d, e) Stokes excitation profiles of the bands at 1522 (d) and 1156 $cm^{-1}$ (e). (f, g) Intensity ratios (the intensity of the 1522 $cm^{-1}$ band divided by that of the 1156 $cm^{-1}$ band): anti-Stokes (f) and Stokes (g). In b−g, dots and solid curves represent the observed points and simulated curves, respectively. Parameters used for the simulation (eqs 8−10) are as follows: 0−0 transition energy = 20 200 $cm^{-1}$; $\Delta_1 = 1.1$; $\Delta_2 = 0.9$; $\Gamma = 250$ $cm^{-1}$; $\nu_{IH} = 450$ $cm^{-1}$.

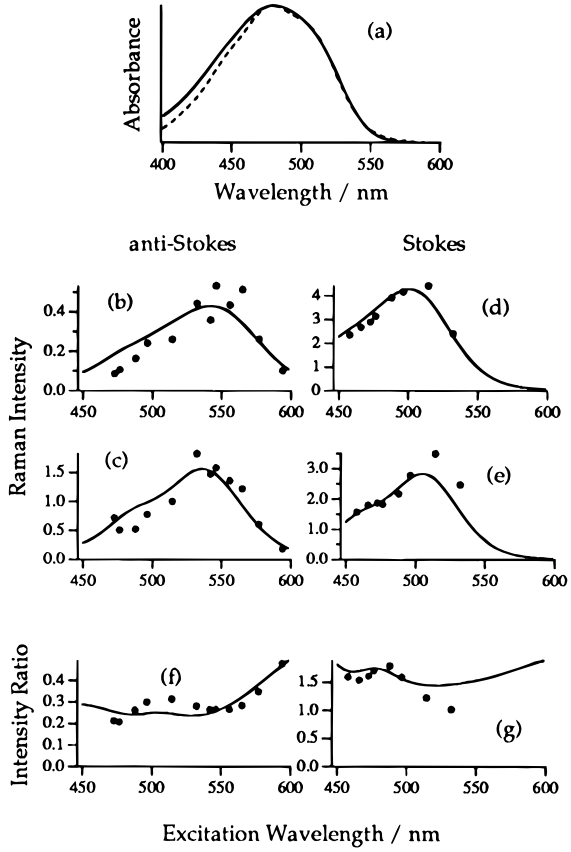


**Figure 3.** Electronic absorption spectrum and Raman excitation profiles of canthaxanthin in benzene solution. (a) Electronic absorption spectrum: observed (solid curve) and simulated (broken curve). (b, c) Anti-Stokes excitation profiles of the bands at 1521 (b) and 1158 $cm^{-1}$ (c). (d, e) Stokes excitation profiles of the bands at 1521 (d) and 1158 $cm^{-1}$ (e). (f, g) Intensity ratios (the intensity of the 1521-$cm^{-1}$ band divided by that of the 1158-$cm^{-1}$ band): anti-Stokes (f) and Stokes (g). In b−g, dots and solid curves represent the observed points and simulated curves, respectively. Parameters used for the simulation (eqs 8−10) are as follows: 0−0 transition energy = 19 600 $cm^{-1}$; $\Delta_1 = 1.1$; $\Delta_2 = 0.9$; $\Gamma = 200$ $cm^{-1}$; $\nu_{IH} = 700$ $cm^{-1}$.

higher than 2000 $cm^{-1}$ are very small at room temperature. In addition, high-frequency Raman bands are generally broad, so that peak intensities are weak.

The signal-to-noise ratios of the Stokes and anti-Stokes bands in Figure 1 are sufficient to discuss the excitation-wavelength dependence of their intensities. The Stokes and anti-Stokes REPs of the C═C and C−C stretching bands are plotted in Figures 2 and 3 for $\beta$-carotene and canthaxanthin, respectively, together with their electronic absorption spectra. The Raman intensities relative to those of the internal intensity reference were determined according to the method described in the Analysis section. The Stokes REPs of $\beta$-carotene (Figure 2d,e) agree well with those reported previously.[3,4,7,8] For example, the intensity of the C═C stretching band is much stronger than that of the C−C stretching band in the wavelength region of the 1−0 absorption maximum (∼465 nm). This is likely to be due to an interference effect among Raman tensor components with different virtual states.

In the anti-Stokes REPs in Figure 2, the peaks are found at longer wavelengths in comparison with the corresponding Stokes REPs. Essentially the same observation was reported for the low-frequency vibrational modes of cytochrome *c*.[13] This is explained as follows. Equation 8 applies to both the Stokes and anti-Stokes processes, except that $\Delta E_{vi}$ for the anti-Stokes process is smaller than that for the corresponding Stokes process by the absolute energy difference between the initial and final states. Consequently, if contributions from hot transitions (see later) are disregarded, the REP of an anti-Stokes Raman band should be shifted from that of the corresponding Stokes Raman band to a longer wavelength by a difference corresponding to the Raman shift. The observations shown in Figure 2 are consistent with this theoretical prediction.

It has been reported[20] that the anti-Stokes Raman bands of *trans*-stilbene in the $S_1$ state are observed clearly when the anti-Stokes Raman spectrum is excited at a wavelength longer than the maximum of the transient electronic absorption of the $S_1$ state. Such an observation may be partly explained in terms of the shift of the anti-Stokes excitation profile to a longer wavelength mentioned above.

Next, we compare the observed Stokes and anti-Stokes REPs with those simulated by the formula given in the previous section. The common intensity scale is applied to the Stokes REPs of the 1522 and 1156 $cm^{-1}$ bands. Since the anti-Stokes intensity depends on the initial population of the vibrationally excited state, an independent intensity scale is used for the simulation of each Raman band; the calculated intensity is multiplied by a scaling factor, which is determined by the least-squares fit to each experimental excitation profile. This scaling factor reflects the Boltzmann distribution of molecules in the vibrationally excited levels of each mode. As is shown in Figure 2b−e, the observed REPs are reproduced by simulation to a

satisfactory degree in view of the fact that the observed REPs were determined in the manner described in the Analysis section.

To compare the observed and simulated REPs more quantitatively, the ratios of the intensities of the band at 1522 $cm^{-1}$ to those of the band at 1156 $cm^{-1}$ are plotted in Figure 2f,g, for both the anti-Stokes and Stokes Raman processes. These plots are free from errors arising from the separation of the intensity of the benzene 992 $cm^{-1}$ band used as the internal intensity reference and that of the 1000 $cm^{-1}$ band of $\beta$-carotene. The simulated Stokes intensity ratios are compared with the observed ones without any scaling factor, while the anti-Stokes intensity ratios are multiplied by a scaling factor, which was determined by the least-squares method (in an ideal case, this scaling factor corresponds to the ratio of the scaling factors used to simulate REPs of the bands at 1522 and 1156 $cm^{-1}$). As is seen in Figure 2f,g, vibrational structures reflecting the Franck−Condon factors are located in the wavelength region between 570 and 450 nm for the anti-Stokes process and in the region between 480 and 450 nm for the Stokes process. Such detailed features of the intensity-ratio profiles are satisfactorily reproduced by the simulated curves, except that a deviation from the simulated curve is found for the observed point at ∼530 nm in Figure 2g. This may be due, at least partly, to larger errors in intensity measurements in the long-wavelength region where the excitation wavelength approaches an off-resonant condition. Another origin of the deviation may lie in the breakdown of the mathematical model of the vibronic band shape, for which we have adopted a simple convolution of a Lorentzian (for homogeneous band shape) and a Gaussian (inhomogeneous). This model function may not be a good approximation in the tail of the vibronic band. In addition, it gives weak Raman intensities in the longer-wavelength side of the lowest-energy vibronic component. Since observed and simulated relative intensities of the two Raman bands are compared in Figure 2g, a serious discrepancy between the two is found in this region, in spite of the apparently good agreement in the REP of each band (Figure 2d,e).

The best-fit parameters of potential displacements, $\Delta_1$ (for the C═C stretch) and $\Delta_2$ (for the C−C stretch), are 1.1 and 0.9, respectively, which are consistent with those obtained in the previous studies.[3−10] From the scaling factor of the anti-Stokes intensity ratio, the vibrational temperature under the Boltzmann distribution is estimated to be ∼260 K, which agrees with room temperature within experimental uncertainty. The observed and calculated electronic absorption spectra shown in Figure 2a agree reasonably with each other.

In a similar way, the REPs and electronic absorption spectrum of canthaxanthin in benzene solution are analyzed, and the results are shown in Figure 3. The simulations satisfactorily reproduce the observed REPs and the electronic absorption spectrum, with almost the same values of the parameters of potential displacements, $\Delta_1$ and $\Delta_2$, as those obtained for $\beta$-carotene. Good agreement between the observed and calculated results is obtained only when the inhomogeneous broadening parameter is set at a considerably larger value than that used for $\beta$-carotene, as is also expected from the broad feature of the electronic absorption. The vibrational temperature estimated from the anti-Stokes intensity ratio is ∼290 K, which again agrees well with room temperature. In a similar way as for $\beta$-carotene, a deviation from the simulated curve is found for the observed point at ∼530 nm in Figure 3g, but such discrepancy is not essential for the discussion in the following subsection.

The quality of the observed anti-Stokes REPs in the present study (except for the intensity-ratio profiles) is not very high because of the numerical treatments for separating overlapping solvent and solute contributions. However, for those cases where such a problem does not exist, observed anti-Stokes REPs may be more quantitatively compared with theoretical ones.

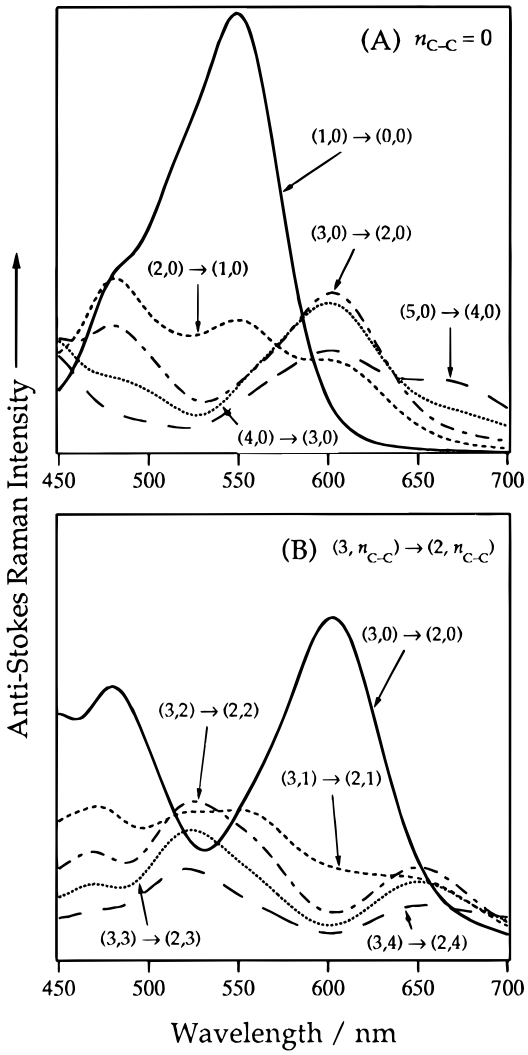


**Figure 4.** Anti-Stokes Raman excitation profiles of transitions of the C═C stretch from various initial levels calculated for canthaxanthin. (A) Anti-Stokes Raman excitation profiles calculated for various initial quantum numbers of the C═C stretch ($n_{C=C}$) with the initial quantum number of the C−C stretch ($n_{C-C}$) being fixed at 0. (B) Anti-Stokes Raman excitation profiles calculated for the transitions from $n_{C=C} = 3$ to 2 with various $n_{C-C}$ values.

**Method of Determining the Energy Levels on which Vibrationally Excited Transients Are Populated.** We have shown above that the Stokes and anti-Stokes REPs of the two carotenoids are quantitatively described by the Franck−Condon model (the Albrecht A term). From the previous studies,[4,7−10] it is known that the observed intensities of overtone and combination Stokes Raman bands are also explained quantitatively by the same model. It is reasonable to consider that similar calculations would lead to a prediction of the REP (in either the Stokes or anti-Stokes side) of a hot band, i.e., a Raman band arising from the initial and final states, neither of which is the ground vibrational state. If an accurate REP is experimentally obtained, the initial state may be identified, in principle, by comparing the observed REP with results calculated for various initial and final states.

REPs calculated for some anti-Stokes hot bands of the C═C stretching vibration of canthaxanthin are shown in Figure 4, where various initial and final states for the Franck−Condon

active C=C and C−C stretches, specified by ($n_{C=C}$, $n_{C-C}$) where *n* refers to the vibrational quantum number, are considered. Each REP in Figure 4A is characteristic of the initial state involved. For example, the REP of the fundamental (1,0) → (0,0) process has neither a peak nor a shoulder in the wavelength region longer than its strongest peak at ∼550 nm, while those of hot-band processes have at least one peak or shoulder in that region. The following features are noted in the calculated REPs.

As noted above, the (1,0) → (0,0) process in Figure 4A has only one peak at ∼550 nm. In the (2,0) → (1,0) process, the peak intensity at ∼550 nm decreases to a large extent, and a peak and a shoulder grow at ∼480 and ∼600 nm, respectively. The intensity at ∼550 nm further decreases in the (3,0) → (2,0) process. In the (4,0) → (3,0) and (5,0) → (4,0) processes, new peaks or shoulders become observable in the even longer (and shorter, not shown in Figure 4A) wavelength regions. To summarize, the REPs of the ($n_{C=C}$,0) → ($n_{C=C}$−1,0) processes (except for $n_{C=C}$ = 1) have peaks or shoulders on the shorter- and longer-wavelength sides of the (1,0) → (0,0) maximum, which spread to shorter and longer wavelengths, respectively, with increasing initial $n_{C=C}$.

In Figure 4B, features similar to the cases in Figure 4A are noticed for the (3,0) → (2,0) process and the (3,$n_{C-C}$) → (2,$n_{C-C}$) processes ($n_{C-C} \neq 0$). The (3,0) → (2,0) process has two peaks at ∼600 and ∼480 nm. In the (3,1) → (2,1) process, the intensities at ∼600 and ∼480 nm decrease and, instead, other peaks and shoulders appear on the shorter- and longer-wavelength sides of the (3,0) → (2,0) peak at ∼600 nm (at ∼550 and ∼650 nm) and also on the shorter- and longer-wavelength sides of the peak at ∼480 nm (∼470 and ∼520 nm). In the (3,2) → (2,2) process, the two peaks of the (3,1) → (2,1) process at ∼550 and ∼520 nm merge to form a clear peak at ∼525 nm, and the peak at ∼650 nm becomes prominent. For higher values of $n_{C-C}$, REPs spread to shorter and longer wavelengths. Such a tendency is similarly observed for other $n_{C=C}$ transitions such as the (4,$n_{C-C}$) → (3,$n_{C-C}$) process. To summarize, the REPs of the ($n_{C=C}$,$n_{C-C}$) → ($n_{C=C}$−1,$n_{C-C}$) processes have peaks (or shoulders) on both the longer and shorter wavelength sides of the ($n_{C=C}$,0) → ($n_{C=C}$−1,0) peaks; they spread to both the longer- and shorter-wavelength sides of the ($n_{C=C}$,0) → ($n_{C=C}$−1,0) peaks with increasing $n_{C-C}$.

Such features in the REPs may be utilized for the assignment of hot bands whose initial states are not identified. Recently, it has been reported by several groups that anti-Stokes Raman bands, which are attributable to vibrationally hot molecules generated by photoexcitation, are observed in pump−probe Raman spectra.[12,20−27] In these studies, however, little information has been obtained about the energy states of the hot molecules. It is important to know vibrational quantum numbers of levels on which such vibrationally excited molecules are populated, to discuss the mechanism of vibrational relaxation. The method proposed in this paper may provide useful information on this issue. In this paper, a simple three-mode Franck−Condon model was adopted to simulate the observed REPs. More advanced treatments including various perturbations, such as the effects of low-frequency modes,[23] may be needed in applying the present method to real problems.

In the paper following this one,[27] the present method will be applied to the study of vibrationally excited transients of canthaxanthin.

## References and Notes


(1) Albrecht, A. C. *J. Chem. Phys.* **1961**, *34*, 1476.
(2) Tang, J.; Albrecht, A. C. In *Raman Spectroscopy*; Szymanski, H. A., Ed.; Plenum Press: New York, 1970; Vol. 2, p 33.
(3) Inagaki, F.; Tasumi, M.; Miyazawa, T. *J. Mol. Spectrosc.* **1974**, *50*, 286.
(4) Sufrà, S.; Dellepiane, G.; Masetti, G.; Zerbi, G. *J. Raman Spectrosc.* **1977**, *6*, 267.
(5) Lukashin, A. V.; Frank-Kamenetskii, M. D. *Chem. Phys.* **1978**, *35*, 469.
(6) Siebrand, W.; Zgierski, M. *J. Chem. Phys.* **1979**, *71*, 3561.
(7) Ho, Z. Z.; Hanson, R. C.; Lin, S. H. *J. Chem. Phys.* **1982**, *77*, 3414.
(8) Okamoto, H.; Saito, S.; Hamaguchi, H.; Tasumi, M.; Eugster, C. H. *J. Raman Spectrosc.* **1984**, *15*. 331.
(9) Sue, J.; Mukamel, S.; Okamoto, H.; Hamaguchi, H.; Tasumi, M. *Chem. Phys. Lett.* **1987**, *134*, 87.
(10) Sue, J.; Mukamel, S. *J. Chem. Phys.* **1988**, *88*, 651.
(11) Torii, H.; Tasumi, M. *J. Chem. Phys.* **1994**, *101*, 4496.
(12) Hayashi, H.; Brack, T. L.; Noguchi, T.; Tasumi, M.; Atkinson, G. H. *J. Phys. Chem.* **1991**, *95*, 6797.
(13) Schomacker, K. T.; Bangcharoenpaurpong, O.; Champion, P. M. *J. Chem. Phys.* **1984**, *80*, 4701.
(14) Hamaguchi, H.; Harada, I.; Shimanouchi, T. *Chem. Lett.* **1974**, 1405.
(15) Watanabe, J.; Kinoshita, S.; Kushida, T. *J. Chem. Phys.* **1987**, *87*, 4471.
(16) Champion, P. M.; Albrecht, A. C. *Annu. Rev. Phys. Chem.* **1982**, *33*, 353.
(17) See, for example, Dirac, P. A. M. In *The Principles of Quantum Mechanics*, 4th ed.; Oxford University Press: Oxford, 1958; p 244.
(18) Saito, S.; Tasumi, M.; Eugster, C. H. *J. Raman Spectrosc.* **1983**, *14*, 299.
(19) See, for example: Fischer, G. In *Vibronic Coupling*; Academic Press: New York, 1984; p 125.
(20) Matousek, P.; Parker, A. W.; Toner, W. T.; Towrie, M.; de Faria, D. L. A.; Hester, R. E.; Moore, J. N. *Chem. Phys. Lett.* **1995**, *237*, 373.
(21) Brack, T. L.; Atkinson, G. H. *J. Phys. Chem.* **1991**, *95*, 2351.
(22) Doig, S. J.; Reid, P. J.; Mathies, R. A. *J. Phys. Chem.* **1991**, *95*, 6372.
(23) Shreve, A. P.; Mathies, R. A. *J. Phys. Chem.* **1995**, *99*, 7285.
(24) Phillips, D. L.; Rodier, J.-M.; Myers, A. B. *Chem. Phys.* **1993**, *175*, 1.
(25) Sato, S.; Kitagawa, T. *Appl. Phys. B* **1994**, *59*, 415.
(26) Nakabayashi, T.; Okamoto, H.; Tasumi, M. *J. Raman Spectrosc.* **1995**, *26*, 841.
(27) Nakabayashi, T.; Okamoto, H.; Tasumi, M. *J. Phys. Chem. A* **1997**, *101*, 3494.